nature geoscience

SUPPLEMENTARY INFORMATION

DOI: 10.1038/NGEO2063

Mapping the density of Earth's mantle using satellite-derived gravity gradients

1. The gravitational gradient anomalies

By sensing tiny differences of acceleration in three orthogonal directions, GOCE measures the six components of the Earth's gravity gradient tensor, out of which five are independent. This symmetric trace-free tensor, which entries are the second-order spatial derivatives of the gravity potential, describes the curvature of the equipotential surfaces (1). Four of its components are determined from GOCE with the extreme accuracy of 10 to 20 milliEötvös/$\sqrt{Hz}$ (1 Eötvös = 10^{-9} s^{-2}) in the 5-100 mHz measurement bandwidth (1), corresponding to spatial scales comprised between 740 and 40 km. The GOCE gradients are measured in the instrument reference frame, which means that the direction of differentiation changes according to the satellite orientation. Using a GOCE orbit-based gravity field model to account for the less precise components of the tensor and for the longest wavelengths, the GOCE High-level Processing Facility computes enhanced gradients in the Local North Oriented Frame (LNOF) (2,3), a local frame with origin at the satellite center of mass and with axes oriented in the North, West and radial directions (Figure S1). We used these Level 2 LNOF gradient packages as provided by ESA, spanning the period from 31/10/2009 to 31/03/2011. We obtained about 28 millions data per component, with a level of precision estimated to 10 to 60 milliEötvös for the LNOF diagonal components in the Level 2 data packages. Averaging over 2.5 months on 1° x 1° spatial blocks, which corresponds to about 100 data per block, leads to an error estimate at the level of a few milliEötvös.

DOI: 10.1038/NGEO2063

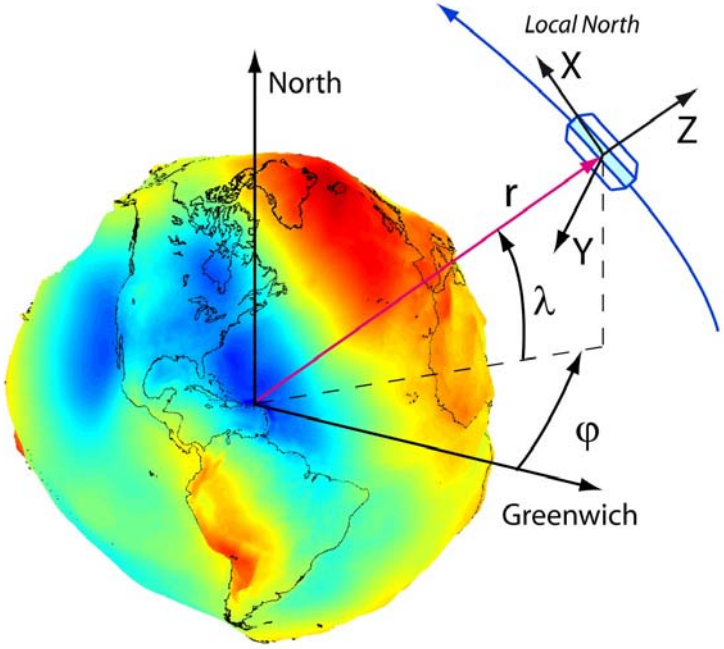

Fig. S1: The Local North-Oriented Frame, indicated by the (X, Y, Z) directions, and with origin located at the satellite center of mass, of spherical geocentric coordinates (r, θ, φ). The Earth's geoid shape, computed from the DIR-R3 model (13), is represented in color (its deviation to the ellipsoid is amplified).

We defined anomalies by subtracting from these data the effect of a reference Earth's model, with an interior structure given by the Preliminary Reference Earth Model at a reference period 1 s (Table 1 of reference 4). We computed the low-degree spherical harmonics expansion of the associated gravitational potential as given in (5), where the hydrostatic, self-gravitating equilibrium of a rotating, radially layered spherical Earth is solved. Multiplying these coefficients with those determined from the computation of the second-order spatial derivatives of the spherical harmonics in the LNOF frame, we obtained the model gradients that we subtracted from the data. We computed the spherical harmonics derivatives at each orbit position following (6), in rectangular coordinates, avoiding singularities at poles (even if these areas are devoid of measurements due to the orbit geometry). We finally gridded the resulting anomalies with a 0.25° step in latitude and longitude using the GMT software (7). Because a physical Earth model is used to define the reference, these gradient anomalies can be used to investigate Earth's structure at all spatial scales. Only the diagonal components are shown in this work but the V_{xz} component can also be used.

The quality assessment of the gradients in the LNOF frame has been done through comparisons with modelled ones from previously existing global gravity models, after filtering in the measurement bandwidth, and did not show trackiness effects that could generate directional artefacts (3). Direct comparisons of the GOCE geoid models with previously existing ones, not including any GOCE data, do not exhibit any trackiness (13). Finally, the good consistency between the gradient anomalies we built, and the predictions from the mantle model, as well as the absence of any significant systematic pattern in our maps, rather indicates that the possible striping artefacts remain small as compared to the discussed physical signals.

2. The lithospheric contribution

We computed the gravitational gradients of a simple lithosphere model at hydrostatic equilibrium, in order to assess its contribution at large scale to the observed gravitational gradients. For that, we supposed a local compensation of the topographic load by the Airy model, and we estimated the depth of the Moho h_c by solving the following equation:

$$(\rho_m - \rho_i)h_i + (\rho_m - \rho_w)h_w + (\rho_m - \rho_s)h_s + (\rho_m - \rho_c)h_c + (\rho_m - \rho_l)h_l - \rho_m h_t = K$$

where K is a constant, ρ_m, ρ_l, ρ_c, ρ_s, ρ_w and ρ_i are the densities of the asthenospheric and lithospheric mantle, oceanic or continental crust, sediments, water and ice, taken to ρ_m = 3300 kgm^{-2}, ρ_l = 3330 kgm^{-2}, ρ_c = 2800 kgm^{-2}, ρ_w = 1020 kgm^{-2} and ρ_i = 917 kgm^{-2}, and h_l, h_t, h_c, h_s, h_w, h_i are the thicknesses of the lithosphere, the topography above the geoid, the thicknesses of the crust, sediment layers, sea water and ice. For sediments, ρ_s and h_s are given by the Global Digital Map of Sediment Thickness (8). Values of h_t, h_w, h_i are given by the ETOPO1 grid (9), and the lithospheric thickness h_l is given by (10). The above equation cannot be solved uniquely due to the constant K indetermination. In order to solve the constant and the equation, we added a constraint on the mean oceanic crust thickness, which is well known to be about 6-7 km (11). In practice here, the equation was solved iteratively, aiming at a typical value of 7 km for the mean oceanic crust thickness. We then computed the gravitational potential of the obtained lithosphere model in spherical geometry by summing the contributions of superimposed 1 km thick radial layers, under the hypothesis of thin layers. This assumption is valid at the GOCE spatial resolution, and allows to link the spherical harmonics expansion of the layer mass load, expressed as a surface load at the center of the layer, to the spherical harmonics expansion of the

DOI: 10.1038/NGEO2063

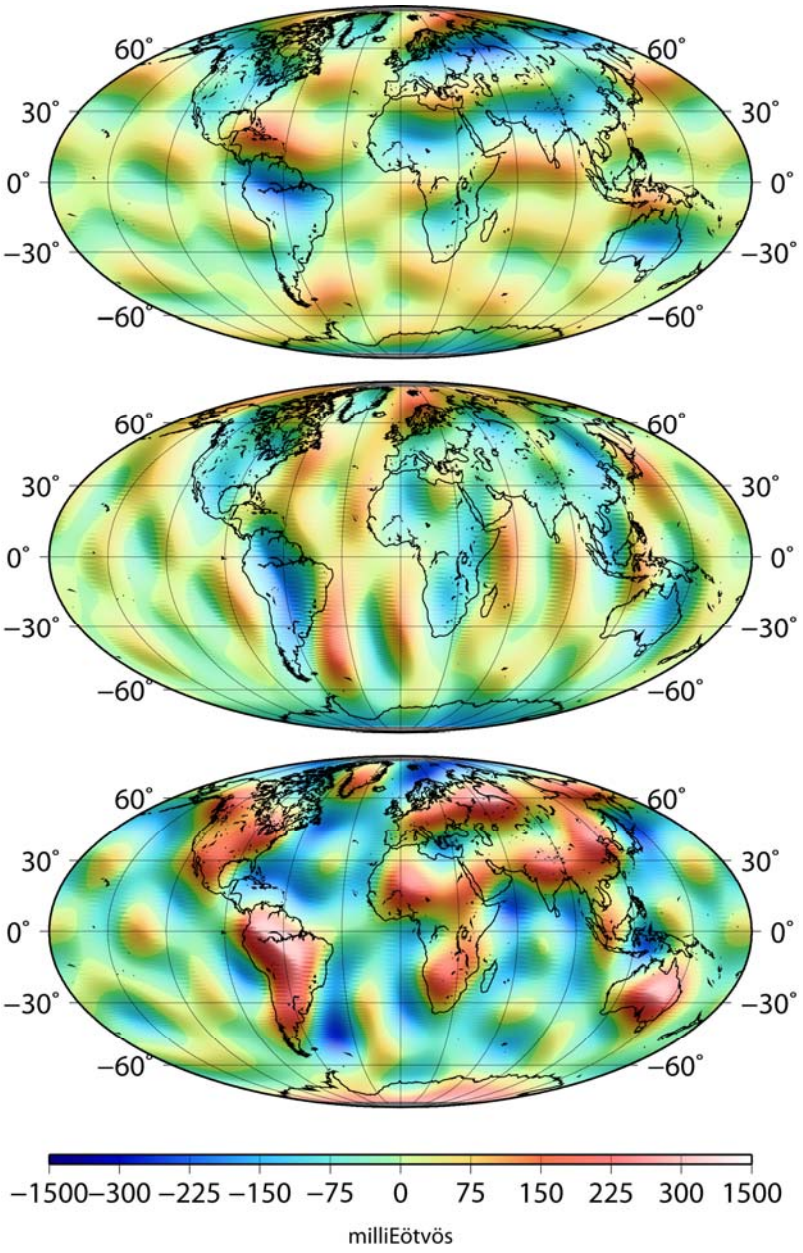

Fig. S2: Maps of the large-scale spatial variations of the second-order derivatives in the *X*/North (*top*), *Y*/West (*middle*) and *Z*/radial Up (*bottom*) directions of the gravity potential associated to the isostatic lithosphere model, along GOCE orbit, in milliEötvös.

associated Newtonian potential. We finally derived the gravitational gradients by multiplying the obtained spherical harmonics coefficients with the second-order derivatives of the spherical harmonics along the satellite orbits, as explained above. Their large-scale

component, at the resolution of the investigated mantle dynamics model (spherical harmonics degree 12), is shown on Figure S2. At large spatial scales, we thus confirm that only little signal is found in the *XX*/*YY* components as compared to what we obtained in the satellites gradients maps and in the mantle model, and that the geographical variations of the lithospheric gradients are dominated by the ocean/continent dichotomy, mostly visible in the *ZZ* component.

3. Sensitivity to mass anomalies in the mantle

Here, we describe the computation of the gravitational gradients along the GOCE orbit due to thin slab-shaped and flat spherical caps mass anomalies, both with 80 kgm^{-3} density contrast to PREM. While such dynamic response functions are usually computed, on the geoid, for individual spherical harmonics (12), here we consider regional distributions of masses. The slab elements are 4500 km long and 100/400 km wide, parallel to the present-day North-America subduction. The caps diameters are equal to 4000 km and 6000 km. The slabs and caps thickness is set to 200 km. We first computed the spherical harmonics expansion of the geoid effect of the mass anomaly. For that, we used the spherical harmonics expansions of the cap/slab mass anomalies at each radius, and from that we derived and summed the spherical harmonics expansion of the direct Newtonian attraction potential and of the Earth's visco-elastic deformation potential, up to spherical harmonics degree/order 75. Then, we obtained the gravitational gradients along the orbit by differentiation of the spherical harmonics.

Fig. S3 shows the variations of the thin slabs gradients anomalies amplitude at the center of the slab, as a function of the slab depth. Masses in the upper part of the lower mantle lead to large central positive (resp. negative) *ZZ* (resp. *XX*, *YY*) anomalies, always above the noise level - not larger than a few milliEötvös at 1° resolution - with a maximum sensitivity above 1600 km depth. Gradients oscillations change sign when the slab reaches the upper mantle, and their tripole shape delineates more and more closely the slab borders as depth decreases. Fig. S4 shows the variations of the spherical cap gradients anomalies amplitude at the center of the cap, as a function of the cap depth. Above 1700 km depth, the cap geometry is resolved and large oscillations appear at its edges and dominate the gradient signal. If the cap is not too wide, these oscillations constructively interfere at its center. Below this depth, the pattern of anomaly is made of one smooth lobe, clearly detectable at the level of precision of the observed gravity gradients. This is the reason why, contrary to

DOI: 10.1038/NGEO2063

the geoid, wide, smooth gradient variations can only be attributed to deep sources. In our tests, 4000 km wide caps are detected up to at least 2500 km depth. Note that the non-spherical geometry of orbits leads to an asymmetry in the gradients patterns.

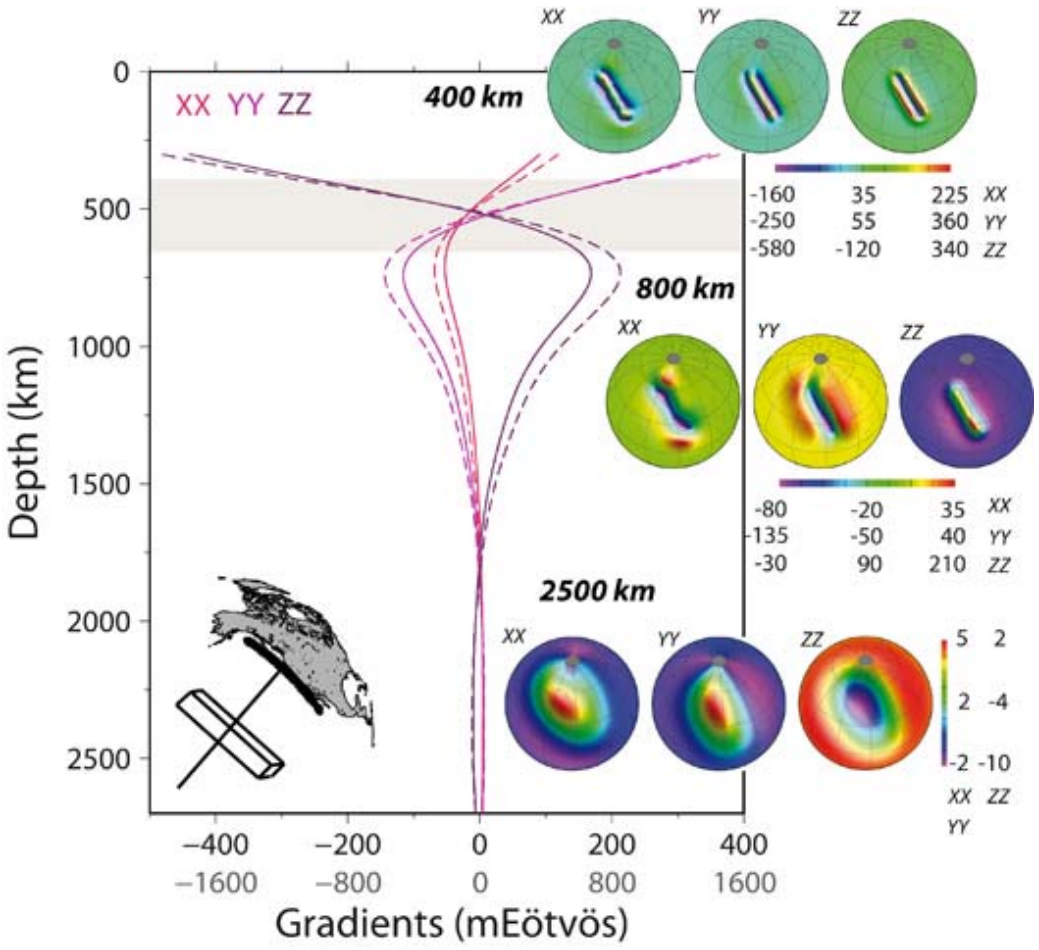

Fig. S3: Gradients sensitivity to subducted slab elements. Graphs of the amplitude, at the GOCE altitude, of the *XX*, *YY* and *ZZ* gravity gradients of 4500 km long and 200 km thick parallelepiped slabs elements parallel to the present-day North American subduction, calculated up to the spherical harmonics degree/order 75 at the point of coordinates (40°*N*, 235°*W*) above the center of the slab, as a function of the depth of the slab element center below Earth's surface. The slab elements are shown on the lower left map. *Solid curves*: case of a 100-km wide slab, with amplitudes given by the black abscissa line; *dashed curves*: case of a 400-km wide slab, with amplitudes given by the grey abscissa line. The transition zone between the upper and lower mantle is delimited by the light gray area. The spatial shape of the associated gradients is represented by maps on the right side, for 100-km wide slab elements at 400, 800 and 2500 km depths. Spatial shapes for the 400-km wide slabs are very similar and thus not shown here.

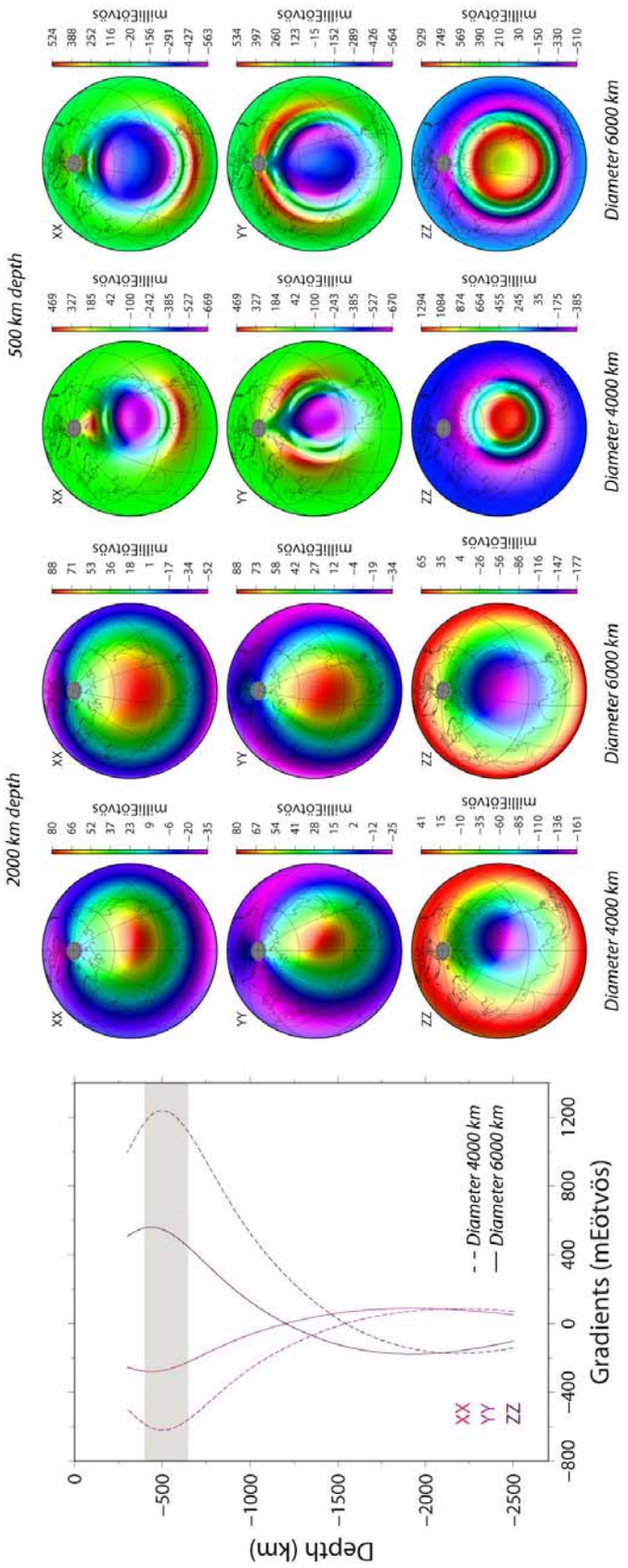

Fig. S4: Graphs of the amplitude at the GOCE altitude of the *XX*, *YY* and *ZZ* gravity gradients of 200-km thick spherical cap mass anomalies, centered at the point of coordinates (45°*N*, 95°*W*), calculated up to the spherical harmonics degree/order 75 above the center of the cap, as a function of the depth of the spherical cap element center below Earth's surface. *Solid curves*: case of a 6000 km diameter cap; *dashed curves*: case of a 4000 km diameter cap. Note that the values obtained for the *XX* and *YY* profiles are identical. The transition zone between the upper and lower mantle is delimited by a light gray area. The spatial shape of the associated gradients is represented by maps on the right side, at 2000 and 500 km depths.

DOI: 10.1038/NGEO2063

References

1. Rummel, R., Yi, W. & Stummer, C. GOCE gravitational gradiometry. *J. Geod.* **85**, 777-790 (2011).
2. Fuchs, M. & Bouman, J. Rotation of GOCE gravity gradients to local frames. *Geophys. J. Int.* **187**, 743-753 (2011).
3. Bouman, J., Fiorot, S., Fuchs, M., Gruber, T., Schrama, E., Tscherning, C., Veicherts, M. & Visser, P. GOCE gravitational gradients along the orbit, *J. Geod.* **85**, 791-805 (2011).
4. Dziewonski, A.M. & Anderson, D.L. Preliminary reference Earth model PREM, *Phys. Earth Planet. Int.* **25**, 297-356 (1981).
5. Chambat, F., Ricard, Y. & Valette, B. Flattening of the Earth: further from hydrostaticity than previously estimated. *Geophys. J. Int.* **183**, 727-732 (2010).
6. Métris, G., Xu, J. & Wytrzyszczak, I. Derivatives of the gravity potential with respect to rectangular coordinates. *Celest. Mech. Dyn. Astr.* **71**, 137-151 (1999).
7. Wessel, P. & Smith, W.H.F. Free software helps map and display data. *EOS Trans. Am. Geophys. Un.* **729**, 441 (1991).
8. Laske, G. & Masters, G. A Global Digital Map of Sediment Thickness. *EOS Trans. Am. Geophys. Un.* **78**, F483 (1997).
9. Amante, C. & Eakins, B.W. ETOPO1 1 Arc-Minute Global Relief Model: Procedures, Data Sources and Analysis. *NOAA Technical Memorandum NESDIS NGDC-24*, 19 pp (2009).
10. Conrad, C.P. & Lithgow-Bertelloni, C. Influence of continental roots and asthenosphere on plate-mantle coupling. *Geophys. Res. Lett.* **33**, L05312 (2006).
11. Turcotte, D.L. & Schubert, G. *Geodynamics* (Cambridge University Press, United Kingdom, 2002), 456 pp.
12. Richards, M.A. & Hager, B.H. Geoid anomalies in a dynamic Earth. *J. Geophys. Res.* **89**, 5987-6002 (1984).
13. Pail, R., *et al.* First GOCE gravity field models derived by three different approaches. *J. Geod.* **85**, 819-843 (2011).